JOURNAL OF GEOPHYSICAL RESEARCH, VOL. 113, D21111, doi:10.1029/2008JD010390, 2008

Surface energy balance in the ablation zone of Midtdalsbreen, a glacier in southern Norway: Interannual variability and the effect of clouds

R. H. Giesen,[1] M. R. van den Broeke,[1] J. Oerlemans,[1] and L. M. Andreassen[2,3]

Received 8 May 2008; revised 4 August 2008; accepted 17 September 2008; published 11 November 2008.

[1] We present a record of almost six years of data (2000–2006) from an automatic weather station (AWS) in the ablation zone of Midtdalsbreen, a glacier in southern Norway. Measured incoming longwave radiation is used to estimate cloudiness, revealing that high cloud fractions occur almost 50% of the time in all seasons. Measured wind speeds and humidity are higher for cloudy conditions, especially in winter. Net solar radiation dominates the surface energy balance in summer, contributing on average 75% of the melt energy. The turbulent fluxes supply 35% of the melt energy while net longwave radiation and the subsurface heat flux are energy sinks of 8% and 2%, respectively. Although the melt rate is generally larger under clear skies, almost 60% of the melt occurs under cloudy skies, a consequence of the prevailing cloudy conditions. Interannual variability in the total melt is found to be equally determined by variations in the date of ice reappearance and differences in the meteorological conditions during melt. Comparing the results for Midtdalsbreen with measurements from an AWS on Morteratschgletscher, Switzerland reveals that the larger ice ablation on Morteratschgletscher primarily results from an earlier start of the melt season and larger net solar radiation. The energy balance model used in this study is found to be more sensitive to changes in the stability correction than to an order-of-magnitude change in the roughness length for momentum.

Citation: Giesen, R. H., M. R. van den Broeke, J. Oerlemans, and L. M. Andreassen (2008), Surface energy balance in the ablation zone of Midtdalsbreen, a glacier in southern Norway: Interannual variability and the effect of clouds, *J. Geophys. Res.*, *113*, D21111, doi:10.1029/2008JD010390.

1. Introduction

[2] Glaciers in southern Norway experience different climatic fluctuations than glaciers in the European Alps. For example, glacier mass balances in southern Norway were positive in the late 1980s and early 1990s, whereas glaciers in the European Alps had strongly negative mass balances during this period [*Reichert et al.*, 2001]. This difference can be attributed to a strong positive phase of the North Atlantic Oscillation (NAO) in these years, resulting in enhanced westerly flow and increased precipitation in Scandinavia, while the moisture transport toward the Alps was reduced [*Hurrell*, 1995]. In response to the mass surplus, many glaciers in southern Norway advanced in the 1990s [*Andreassen et al.*, 2005]. The advance came to a halt around the turn of the century, currently almost all these glaciers are retreating [*Kjøllmoen et al.*, 2007].

[3] To estimate the response of glaciers to a change in climatic variables, models are needed. An essential part in such models is a realistic description of the interaction between atmospheric fluxes and the glacier surface. Such information can be obtained from glacio-meteorological studies, which have been performed on glaciers spread over the world [e.g., *Ishikawa et al.*, 1992; *Wagnon et al.*, 1999; *Oerlemans*, 2000; *Mölg and Hardy*, 2004; *Konya et al.*, 2004; *Klok et al.*, 2005] and have given insight in the variability in the absolute values of the energy fluxes and their relative importance in the surface energy balance [*Willis et al.*, 2002; *Hock*, 2005]. In the 1950s and 1960s, several detailed glacio-meteorological experiments were conducted on glaciers in southern Norway [*Liestøl*, 1967; *Klemsdal*, 1970; *Messel*, 1971]. These studies have provided important information about the processes governing melt on these glaciers, but interpretation of the results is limited by the short and different measurement periods on the glaciers, the lack of longwave radiation measurements and the simplified treatment of the turbulent fluxes. In the following decades, both the experimental and computational facilities greatly improved. Several extensive studies were carried out on Alpine glaciers, allowing for a detailed analysis of spatial and temporal variability in meteorological variables and the surface energy fluxes on these glaciers [e.g., *Greuell et al.*, 1997; *Oerlemans and Klok*, 2002;

[1] Institute for Marine and Atmospheric Research Utrecht, Utrecht University, Utrecht, Netherlands.
[2] Section for Glaciers, Snow and Ice, Norwegian Water Resources and Energy Directorate, Oslo, Norway.
[3] Department of Geosciences, University of Oslo, Oslo, Norway.

0148-0227/08/2008JD010390$09.00

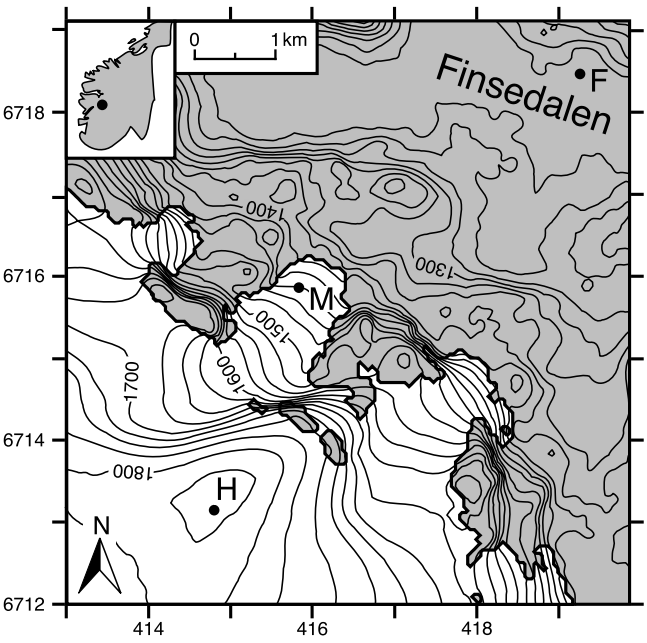

Figure 1. Location and map of Midtdalsbreen in southern Norway. The map shows the locations of the IMAU–AWSs on Midtdalsbreen (M) and the summit of Hardangerjøkulen (H). The AWS Finsevatn (F) is operated by the Norwegian Meteorological Institute. The coordinate system is UTM zone 32 (EUREF89). The map is created from a 1995 digital elevation model by Statens Kartverk, the contour interval is 25 m.

Strasser et al., 2004]. On Norwegian glaciers, no such measurements were done until the early 21st century, when two automatic weather stations (AWSs) were installed on the glaciers Storbreen and Midtdalsbreen in southern Norway. The record from Storbreen was analyzed by *Andreassen et al.* [2008], the measurements from the AWS on Midtdalsbreen form the basis for this paper.

[4] The AWS data cover the period October 2000 to September 2006 and include all standard meteorological variables and the radiation fluxes. Apart from a 39-day data gap in the summer of 2005, the record is continuous. The remaining surface energy fluxes are calculated with an energy balance model [*Van den Broeke et al.*, 2005]. The aim of this paper is to provide insight into the seasonal and interannual variability in meteorological variables, surface energy fluxes and ablation at the AWS site on Midtdalsbreen. Because cloudy conditions prevail on this glacier, we investigate the differences in meteorological variables and the surface energy fluxes under clear and overcast skies. To identify differences between the climate on a Norwegian and an Alpine glacier, the results for Midtdalsbreen are compared to measurements from an AWS on Morteratschgletscher, Switzerland. The uncertainty in the model results is determined by investigating the sensitivity of the energy balance model to changes in the roughness length for momentum and the stability correction.

2. Setting and AWS Description

[5] Midtdalsbreen (60° 34′N, 7° 28′E) is a north-easterly outlet glacier of Hardangerjøkulen, an ice cap on the northwestern border of the Hardangervidda plateau in southern Norway. At approximately 100 km from the Atlantic Ocean, the glacier is situated in the transitional zone between the maritime climate near the coast and the more continental climate further east. The glacier covers an elevation range from 1380 to 1865 m a.s.l. and has an area of 6.7 km^2 (Figure 1). Length change measurements were started at Midtdalsbreen in 1982 [*Andreassen et al.*, 2005]; the net retreat measured until 2006 was 25 m [*Kjøllmoen et al.*, 2007]. Annual mass balance has been measured in 2000 (+1.3 m w.e.) and 2001 (−0.6 m w.e.) [*Kjøllmoen et al.*, 2001, 2003]. A long record of annual winter and summer mass balance is available for Rembesdalsskåka, a southwesterly outlet glacier of Hardangerjøkulen. For the period 1963–2006, the mean net mass balance is +0.08 m water equivalent (w.e.), with a mean winter balance of +2.08 m w.e. and a mean summer balance of −2.00 m w.e. [*Kjøllmoen et al.*, 2007]. For the six years in our AWS record, the mean net balance on Rembesdalsskåka was −0.72 m w.e., a result of both a lower mean winter balance (+1.72 m w.e.) and more ablation (−2.45 m w.e.). Although the summer and winter balances at Rembesdalsskåka and Midtdalsbreen are not directly related because of the different orientations of the glaciers, these numbers indicate that the 6-year meteorological record presented here will not likely represent the climatic mean over the past decades but is associated with a warmer climate with less snow and more melt.

[6] The AWS (M in Figure 1) is situated in the ablation zone of Midtdalsbreen, at an altitude of 1450 m a.s.l., about 400 m from the glacier terminus. At the AWS location, the surface slope is approximately 7° with a north-east aspect. The AWS was installed in October 2000 and is operated by the Institute for Marine and Atmospheric research Utrecht (IMAU). The mast carrying the instruments stands freely on the ice surface. Sensor specifications are listed in Table 1. Air temperature, relative humidity, wind speed, and wind direction are measured at two levels. Temperature and humidity sensors are mounted on the arms at 2.4 and 5.7 m above the ice surface, the measurement level of the wind speed and wind direction sensors is 0.35 m higher. In addition, the upper arm carries a radiation sensor, measuring the four components of the radiation balance (incoming and reflected solar radiation, incoming and outgoing longwave radiation), and a sonic ranger, measuring the distance to the surface. A second sonic ranger is mounted on a tripod, which is drilled into the ice, giving information on both snow accumulation and snow/ice melt. The sonic ranger located in the mast takes over when the other sensor is buried by snow. Readings at ablation stakes around the AWS are used as a reference for the sonic ranger measurements and enable continuation of the surface height record when data from the height sensors is missing. Air pressure is recorded inside the box containing the electronics. Sample time varies per sensor (Table 1), every 30 minutes (average) values are stored in a data logger (Campbell CR10X). Power is supplied by lithium batteries, a solar panel generates energy to ventilate the temperature sensors.

[7] From May to November 2005, a second IMAU–AWS was operational on the summit of Hardangerjøkulen (1860 m a.s.l., H in Figure 1). This AWS measured the same quantities as the AWS on Midtdalsbreen, but at hourly

Table 1. Specifications for the AWS Instruments

Measured Quantity	Sample Interval (minutes)	Instrument	Measurement Range	Accuracy
Air temperature	5	Vaisala HMP45C	−39.2 to +60°C	0.2°C (at +20°C) 0.5°C (at −39.2°C)
Relative humidity	5	Vaisala HMP45C	0.8 to 100%	2% (0 to 90%) 3% (90 to 100%)
Air pressure	30	Vaisala PTB101B	600 to 1060 hPa	0.5 hPa (at +20°C) 2.0 hPa (at −20 to +45°C)
Wind speed	5	Young 05103	1 to 60 m s^{-1}	0.3 m s^{-1}
Wind direction	5	Young 05103	360°	3°
Solar radiation	5	Kipp and Zonen CNR1	0 to 2000 W m^{-2}	10% for daily sums
Longwave radiation	5	Kipp and Zonen CNR1	−250 to +250 W m^{-2}	10% for daily sums
Surface height	30	Campbell SR50	0.5 to 10 m	0.01 m or 0.4%

intervals. Data from this AWS were used to fill the gap in the AWS record from Midtdalsbreen (section 3.6).

3. Data Treatment

3.1. Air Temperature

[8] At times when the solar panel was below the snow surface or malfunctioned for other reasons, the temperature sensors were not aspirated and the measurements had to be corrected for radiation errors. We applied expressions derived from simultaneous measurements with the Vaisala HMP45C and a fine-wire thermocouple at one of the IMAU–AWS sites on Greenland [*Smeets*, 2006]. These expressions give the excess temperature as a function of wind speed and the sum of incoming and reflected solar radiation.

3.2. Humidity

[9] The humidity sensor measures relative humidity with respect to water. These values are too low at air temperatures below the melting point temperature, where relative humidity should be measured with respect to ice. Relative humidities measured under freezing conditions have been corrected by multiplying by the ratio of the saturated water vapor pressures over water and over ice, using an expression by *Curry and Webster* [1999]. Specific humidity has been calculated from relative humidity, air temperature and air pressure.

3.3. Surface Height

[10] The sonic ranger uses the speed of sound at 0°C to determine the distance from the travel time of an ultrasonic sound pulse. At other air temperatures, the measured distance has to be corrected by multiplying by the ratio of the actual speed of sound and the speed of sound at 0°C. Because the temperature profile of the air between the sensor and the surface is not accurately known, we use air temperature measured at the upper mast level as a rough estimate.

3.4. Cloudiness

[11] Cloudiness (n) is not measured directly and was determined following an approach similar to *Van den Broeke et al.* [2006]. Polynomials were fitted through the 5th and 95th percentiles of incoming longwave radiation, binned into air temperature intervals of 1 K. *Van den Broeke et al.* [2006] use net longwave radiation and take 0 W m^{-2} as the upper boundary condition for all temperatures. This is applicable to Antarctic data, but on a melting glacier surface the net longwave radiation is often positive in summer. We obtained a good fit for the upper boundary by applying the Stefan–Boltzmann law with the observed air temperature and unit emissivity. For the lower boundary, a second order polynomial fit the data well. The two polynomials are assumed to represent the minimum and maximum incoming longwave radiation at a given temperature, corresponding to cloudiness values of 0 and 1, respectively. By assuming that cloudiness increases linearly between these minimum and maximum values, the cloud fraction for each half-hourly interval could be calculated from the measurements of air temperature and incoming longwave radiation.

[12] To investigate the variation in atmospheric quantities and energy fluxes for different cloud conditions, we created subsets of the data for clear-sky and overcast conditions. *Van den Broeke et al.* [2006] defined clear-sky conditions to occur when cloudiness values were smaller than 0.3 and overcast conditions were defined as cloudiness values larger than 0.7. Our large data set allowed us to choose the values 0.2 and 0.8, making the difference between the clear-sky and overcast subsets even more distinct. With this definition, 24% of the measurements fell in the clear-sky regime and 44% in the overcast regime.

3.5. Shortwave Radiation

[13] The tilt of the mast varies as a result of forces exerted by the snowpack and differential melting of the ice surface. The envelope of measured half-hourly solar radiation showed noticeable differences between the years and in some periods exceeded the maximum possible irradiance, hence a tilt correction was necessary. The radiation sensor contains a tilt sensor, but this sensor did not function properly. Still, the variation of the tilt with time could be estimated by combining the tilt values obtained from the tilt sensor with tilt angles measured during maintenance visits. Because of the large uncertainty in these estimates, tilting of the sensor increases the uncertainty in the shortwave incoming radiation measurements. A maximum tilt of several degrees in southerly directions is often seen in late spring, when the steel cables that stabilize the mast experience a larger pressure from the snowpack on the up-glacier than on the down-glacier side of the mast. As the tilt only affects direct incoming solar radiation, values are especially overestimated on clear-sky days. In contrast to the other years, the mast was tilted toward the north in 2003 and the tilt was larger (4° to 8°), resulting in an underestimation of incoming solar radiation. Before a correction could be applied, the

fraction of direct solar radiation to the total incoming solar radiation had to be determined. We assumed a linear relation between the fraction of direct solar radiation (f_{dir}) and cloudiness

$$f_{dir} = T_R T_g (1 - n), \quad (1)$$

with $T_R T_g$ a transmission coefficient for Rayleigh scattering and absorption by gases after *Meyers and Dale* [1983]. This coefficient depends on the solar zenith angle and air pressure and makes f_{dir} dependent on the optical depth of the atmosphere. For the Midtdalsbreen data, $T_R T_g$ is 0.86 on average, with a maximum of 0.95. Subsequently, for each 30-minute interval, standard expressions are used to compute the amount of solar radiation incident on a horizontal surface and on a surface with the observed tilt [e.g., *Iqbal*, 1983, chapter 4]. The direct part of the measured incoming shortwave radiation is corrected for the tilt by multiplying by the ratio of these calculated solar irradiance values. In case the AWS site is shaded by surrounding topography, only diffuse radiation reaches the sensor and no correction is applied. After the tilt correction, we have incoming solar radiation on a horizontal surface, i.e., global radiation. In relative numbers, the correction is largest in winter, when the solar zenith angle is large. The largest absolute corrections occur in spring and summer, when insolation is maximum. For more than 90% of the days with a correction applied, the correction affects daily mean incoming solar radiation by values ranging between -10 and $+10$ W m^{-2}. Only in 2003 and the spring of 2005, when the mast was tilted due north and south, respectively, corrections are larger, occasionally exceeding ± 20 W m^{-2}. Even though this correction is based on estimated tilt values, it removes most of the inhomogeneity in incoming solar radiation between the different years.

[14] Half-hourly values of net shortwave radiation were calculated from reflected solar radiation, using the accumulated albedo method [*Van den Broeke et al.*, 2004]. This method removes the effects of a poor cosine response of the radiation sensor at low sun angles on the daily cycle of incoming solar radiation. As we only use daily mean values in this analysis, the effect of this correction is not noticeable.

3.6. Data Gaps

[15] On 18 July 2005, the mast fell down because of the opening of a crevasse under the AWS, resulting in 39 days without usable data. Measurements from the AWS at the summit of Hardangerjøkulen (Figure 1) were used to fill the gap of the AWS on Midtdalsbreen for variables that were well correlated between the two stations. The mean difference in air temperature at the two locations for the period when both stations were operational was added to the air temperature record of the summit station to obtain values for the AWS on Midtdalsbreen. For wind speed we used the ratio of the summed wind speeds at the two AWSs. Incoming shortwave radiation was used without adjustments. For the major part of the gap period, the surface at the lower station was snow-free and is expected to be melting. Hence we used the mean ice albedo from the other years (0.31) to calculate the reflected shortwave radiation and set the emitted longwave radiation to that of a melting surface. Values for relative humidity could not be taken from the summit AWS. At the higher altitude the air was frequently saturated and did not give adequate information to derive humidity values for the lower location. Because of problems with the sensor, the incoming longwave radiation measurements at the upper AWS were unrealistic. For these two variables, we used measurements from an IMAU–AWS (1570 m a.s.l.) on Storbreen, which is located 120 km from Midtdalsbreen [*Andreassen et al.*, 2008]. Data from this AWS generally display simultaneous and similar fluctuations as the data from Midtdalsbreen, which will be discussed in more detail in a subsequent paper. Daily mean values of incoming longwave radiation for Storbreen and Midtdalsbreen, measured for the period 18 July to 25 August in 2002, 2003 and 2006, have a correlation coefficient r of 0.75. The record from Storbreen contains a gap in the summer of 2004, therefore this year was excluded. Averaged over the three periods, values are 6 W m^{-2} lower on Midtdalsbreen with a standard deviation σ for daily averages of 15 W m^{-2}. Daily mean relative and specific humidity on the two glaciers are correlated with $r = 0.76$ and $r = 0.81$, respectively. Relative humidity values are 0.4% lower on Midtdalsbreen ($\sigma = 6.7\%$ for daily values), while specific humidity is 0.19 g kg^{-1} higher ($\sigma = 0.51$ g kg^{-1} for daily values). We used half-hourly relative humidity from Storbreen without adjustments, then specific humidity calculated for Midtdalsbreen is on average 0.15 g kg^{-1} higher than specific humidity calculated for Storbreen due to higher air temperatures on Midtdalsbreen. For incoming longwave radiation we shifted the Storbreen record by the mean difference between the two AWSs. Alternatively, the gap could be filled with synthetic data produced by using information from the other years in the Midtdalsbreen AWS record. The advantages of using measurements from another AWS are that anomalies with respect to the other years in the record are preserved and realistic inter-daily fluctuations are incorporated. Although the relative humidity and incoming longwave radiation records from Storbreen and Midtdalsbreen are not highly correlated and differences between the locations need to be dealt with, correlations would be even lower if the other years in the Midtdalsbreen record were used to fill the gap. Nevertheless, results obtained for this period should be interpreted with care.

[16] The sensors at the lower measurement level were buried by snow in two out of the six winters. The sonic ranger on the tripod was also buried in the snowpack during several winter seasons and melted out at the end of several summer periods. Furthermore, sonic ranger data are missing for shorter periods during the remainder of the year. Small gaps in the surface height record were filled by linear interpolation between values at the start and end of the gap; for larger gaps in the melt season we used melt values calculated from the surface energy balance (see section 4), combined with stake readings. On 1 February 2001 the sonic ranger on the tripod was buried by snow, while the snowpack was not thick enough to be detected by the sonic ranger in the mast until 4 March. This gap was filled by using precipitation measured at Liset (748 m a.s.l.), a Norwegian Meteorological Institute (NMI) precipitation station located 20 km south-west of the AWS site on

Midtdalsbreen. We multiplied the cumulative precipitation record from Liset for the gap period by the ratio of the observed snow depth difference between the begin and end date of the gap and the total precipitation measured at Liset during this period. Air temperature at the AWS site on Midtdalsbreen was always below 0°C during the gap period, hence all recorded precipitation was assumed to fall as snow. Although this method is simple, it produces a more realistic temporal record of accumulation than linear interpolation between the snow depth values surrounding the gap.

4. Surface Energy Balance

[17] The energy balance at the glacier surface can be written as:

$$Q = S_{\text{in}} + S_{\text{out}} + L_{\text{in}} + L_{\text{out}} + H_{\text{sen}} + H_{\text{lat}} + G \quad (2)$$

$$= S_{\text{net}} + L_{\text{net}} + H_{\text{sen}} + H_{\text{lat}} + G, \quad (3)$$

where Q is melt energy ($Q = 0$ if the surface temperature is below the melting point), S_{in} and S_{out} are incoming and reflected solar radiation, L_{in} and L_{out} are incoming and outgoing longwave radiation, H_{sen} and H_{lat} are the sensible and latent heat fluxes and G is the subsurface heat flux. Net solar radiation and net longwave radiation are written as S_{net} and L_{net}. All fluxes are defined positive when directed toward the surface. Heat supplied by rain is neglected, which is justified on glaciers with a considerable mass turnover [*Oerlemans*, 2001]. Penetration of shortwave radiation is not included either. Compared to the other fluxes its contribution to the energy balance is expected to be small.

4.1. Model Description

[18] We have used an energy balance model previously applied to AWS measurements on Antarctica [*Van den Broeke et al.*, 2005, 2006]. The model determines the surface energy balance in equation (2) for a skin layer without heat capacity. S_{in}, S_{out} and L_{in} are taken from the (corrected) measurements, the other fluxes are written as functions of the surface temperature T_{s}. The model time-step is 10 minutes to keep changes in T_{s} between time-steps small and to determine accurately when the surface is melting. To obtain model input for every time-step, the AWS data are linearly interpolated between half-hourly values. Using an iterative procedure, the surface energy balance is solved for T_{s}. If T_{s} found by the model is higher than the melting point temperature, T_{s} is set back to 0°C and the excess energy is used for melting. The amount of melt M in meters water equivalent (m w.e.) is calculated by dividing Q by the latent heat of fusion (3.34×10^5 J kg^{-1}) and the density of water (1000 kg m^{-3}).

[19] The turbulent fluxes are calculated with the bulk method, based on differences in wind speed v, potential temperature θ and specific humidity q between a measurement level and the surface. To illustrate the principle of the bulk method and for reference in later sections, the sensible heat flux equations are given below. The latent heat flux equations and details of the model procedure can be found in *Van den Broeke et al.* [2006]. The sensible heat flux is given by

$$H_{\text{sen}} = \rho c_p u_* \theta_*, \quad (4)$$

with ρ the air density and c_p the specific heat capacity of dry air at constant pressure. The turbulent scales of velocity u_* and potential temperature θ_* are computed from [e.g., *Garratt*, 1999]:

$$u_* = \frac{\kappa[v(z_v) - v(z_{0v})]}{\ln(z_v/z_{0v}) - \Psi_{\text{m}}(z_v/L_{\text{MO}})} \quad (5)$$

$$\theta_* = \frac{\kappa[\theta(z_T) - \theta(z_{0T})]}{\ln(z_T/z_{0T}) - \Psi_{\text{h}}(z_T/L_{\text{MO}})}, \quad (6)$$

where κ is the Von Kármán constant (0.4) and z_v and z_T are the measurement levels of wind speed and temperature, respectively. Ψ_{m} and Ψ_{h} are the vertically integrated stability correction functions for momentum and heat, respectively. They are functions of the Monin–Obukhov length scale L_{MO}. Values for the roughness length for momentum z_{0v} were derived from wind speed differences between the AWS upper and lower measurement levels. The criterion $|z/L_{\text{MO}}| < 0.1$ was used to select near-neutral atmospheric conditions, where L_{MO} was estimated by running the model with $z_{0v} = 2$ mm. This criterion largely reduced the set of z_{0v} values for the summer season when the air is generally stably stratified. Strong smoothing of the z_{0v} values revealed an annual cycle with minimum values in mid-winter increasing toward maximum values in summer. As the shape and magnitude of the annual cycle vary largely from year to year, it was not possible to fit a function through the data. Instead, constant values for snow and ice surfaces were determined by the median values of the natural logarithm of z_{0v}, giving $z_{0v} = 0.13$ mm for snow surfaces (10,890 points) and $z_{0v} = 0.75$ mm for ice surfaces (491 points). The number of points for ice surfaces is low, but the points are distributed over the season and including more points in the data set did not change the value for z_{0v} notably. In section 7.1 we investigate the sensitivity of the model results to the values for z_{0v} and z_{0v}. The roughness lengths for heat z_{0T} and moisture z_{0q} are calculated according to *Andreas* [1987].

[20] On glaciers, katabatic winds often have a wind speed maximum within the first meters above the surface. Assumptions made in Monin–Obukhov similarity theory, on which the bulk method is based, are not valid in the presence of a wind speed maximum. Still, the bulk method has been found to give good results when the measurement level is below the wind speed maximum [*Denby and Greuell*, 2000]. This argument favors the use of measurements made at the lower arm. However, the lower sensors were buried in the snowpack during several winters and had other problems, while the record from the upper sensors is continuous, except for the data gap in 2005. Therefore we use the measurements from the upper level. In combination with the wind speed from the upper measurement level, the stability correction in the model tends to cause an underestimation of the turbulent fluxes under conditions with low

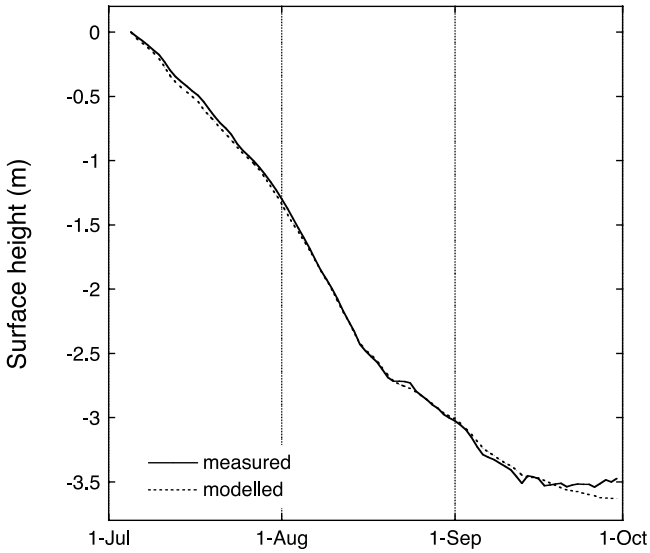

Figure 2. Daily mean values of the surface height measured by the sonic ranger for the summer of 2004 and ice melt calculated with the energy balance model.

wind speeds. Hence, based on a comparison with measurements from the lower level, we limit the flux reduction by the stability correction under stable conditions to one third.

[21] Subsurface heat conduction is computed from the one-dimensional heat-transfer equation for 0.04 m thick layers down to a depth of 20 m. The temperature at the lowest level is assumed to remain stable. The initial temperature profile is generated by running the model in a continuous loop over the measurement period until the 20 m temperature becomes stable within 0.01°C. We found a lower boundary ice temperature of −1.35°C, which is close to the mean annual air temperature. The number of snow layers in the model is determined by dividing the observed snow depth by the model layer thickness. Melt water is routed vertically through the snowpack and refreezes where snow temperatures are below the melting point. When the snowpack is saturated with melt water, the remaining melt water is assumed to run off. Snow density is needed to determine the maximum water content, the amount of refreezing and snow conductivity. Snow density profiles have only been measured occasionally in spring, but the model results show little sensitivity to the exact values used. Hence we use a constant snow density of 500 kg m^{-3}, based on measurements in snowpits around the AWS. The model does not keep track of the changing depth of the snowpack, the record from the sonic ranger is used instead. When the snow has disappeared, input from the height sensor is not needed anymore and model and measurements are independent. For this snow-free period, the melt M computed by the model can be compared with the surface lowering registered by the sonic ranger and the ablation stakes by dividing M by 0.9, the ratio of the ice and water densities used here.

4.2. Model Performance

[22] Comparison of modeled and observed surface temperatures (calculated from measured L_{out}, assuming a surface with unit emissivity) gives an indication of the model performance. The averaged difference between modeled and observed surface temperatures ΔT_s is +0.02°C, with a root-mean-square error (RMSE) of 1.2°C. Given the uncertainties in both the measurements and the energy balance model, this is a good result. Surface temperatures are mainly overestimated on clear-sky winter days and occasional winter days with positive net longwave radiation, possibly due to riming of the incoming longwave radiation sensor. The difference between modeled and measured ice melt (stakes) is +0.4 m ice over the entire six year period. With a total measured ice melt of 24.0 m ice, this is a small difference (<2%). Comparison with the sonic ranger record shows that the model tends to overestimate ice melt when summer snowfalls occurred. As it is difficult to estimate the amount of snow mass added to the surface at such an event, no mass is added in the model while it is included in the measurements. Figure 2 displays measured and modeled ice melt for the summer of 2004, the only summer with a complete sonic ranger record. The good match between modeled and measured surface melt indicates that all relevant processes are included in the model.

5. General Climate Conditions

[23] In this section, we present an overview of the annual mean values (1 January–31 December) and interannual variability of the measured climate variables (Table 2) and describe a selection of the data in more detail. As the records from the sensors at the lower level show several data gaps, measurements from the upper measurement level were used for the analysis. The data were not corrected for the changing measurement height when snow was present as the corrections would generally be small.

5.1. Incoming Solar Radiation and Cloudiness

[24] The upper panel in Figure 3 shows the marked seasonal cycle in daily mean incoming solar radiation. Cloudiness causes the large inter-daily fluctuations. The envelope of the measured radiation is asymmetric with respect to the annual cycle of incoming solar radiation at the top of the atmosphere, suggesting that clouds are more frequent or thicker in late summer and fall than in spring and early summer. The seasonal variation in the occurrence of clear-sky and overcast conditions (Figure 4) indeed shows a larger fraction of clear-sky conditions in spring and more cloudy days in autumn. Multiple reflection between the snow surface and the surrounding slopes may also increase incoming solar radiation in spring. During approximately two months centered around the winter

Table 2. Annual (1 January–31 December) Mean Values of Climate Variables[a]

	2001	2002	2003	2004	2005	Mean
Air temperature (°C)	−2.2	−1.4	−0.7	−1.3	−1.4	−1.4
Relative humidity (%)	83.4	82.1	78.8	83.3	84.2	82.4
Specific humidity (g kg^{-1})	3.41	3.54	3.51	3.56	3.60	3.52
Wind speed (m s^{-1})	6.3	6.4	6.5	7.0	6.8	6.6
Air pressure (hPa)	846.5	848.0	849.2	846.9	848.8	847.9
Cloud fraction	0.60	0.62	0.58	0.62	0.61	0.61
Sky transmissivity	0.49	0.49	0.49	0.48	0.49	0.49
Surface albedo	0.66	0.67	0.68	0.71	0.68	0.68

[a]The year 2006 has not been included, as the data were only available until September 2006.

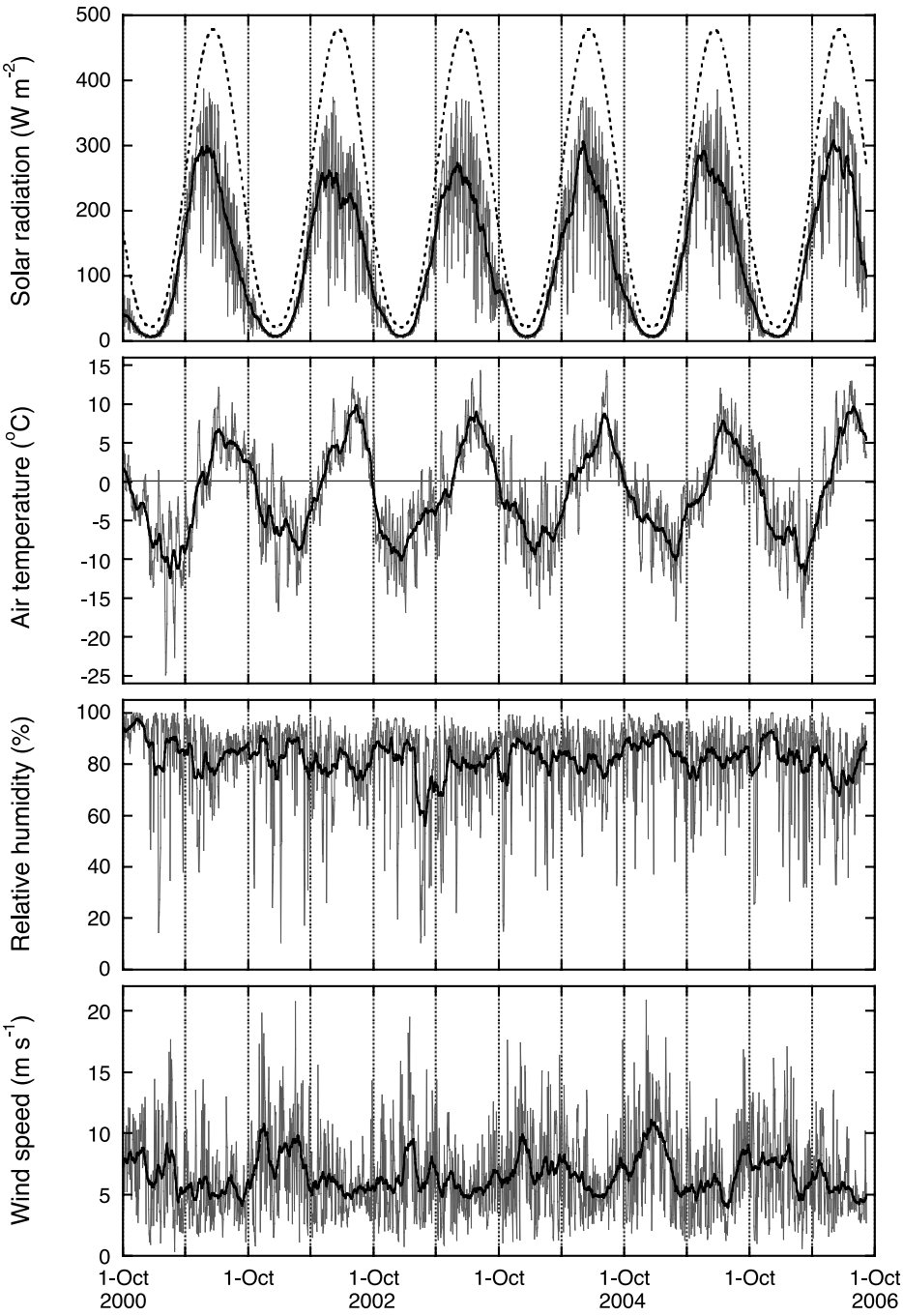

Figure 3. Daily mean values of incoming shortwave radiation, air temperature, relative humidity, and wind speed at the upper measurement level (gray lines) for the period 2 October 2000 to 7 September 2006. The black lines are moving averages over 31 days. The dashed line in the upper panel is incoming solar radiation at the top of the atmosphere.

solstice, the AWS site does not receive any direct sunlight, as the sun is obscured by surrounding topography.

5.2. Air Temperature and Humidity

[25] The annual mean air temperature is −1.4°C (Table 2), with an annual range of typically 15°C. Both the winter of 2000–2001 and the following summer were clearly colder than the other years in the record, with minimum daily mean temperatures as low as −25°C in February 2001 (Figure 3). The summers of 2002 and 2006 were the warmest in the record with mean June–August temperatures of 6.8 and 7.3°C, respectively. The seasonal cycle of air temperature is larger for clear-sky than for overcast conditions (Figure 5). In winter, air temperatures under clear and overcast skies are comparable; from May to September temperatures are higher on clear-sky days when net radiation is larger. Under overcast skies, the difference between air and surface temperature is small, except in summer, when the surface temperature is restricted by the melting point. For clear-sky conditions, the difference between air and surface

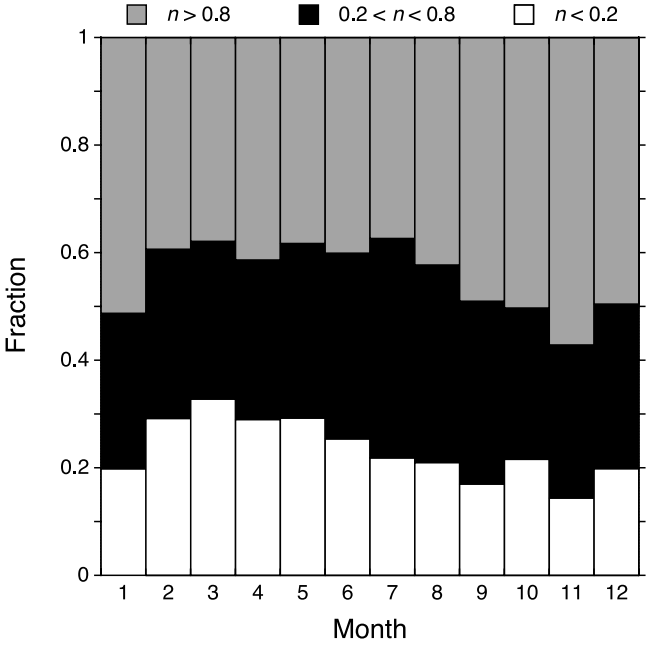

Figure 4. Monthly occurrence of clear-sky ($n < 0.2$) and overcast ($n > 0.8$) conditions.

temperature is also large in winter, when incoming solar radiation is small and the surface is cooled by negative net longwave radiation.

[26] The air on Midtdalsbreen is humid, with daily mean relative humidities larger than 80% for more than 70% of the time (Figure 3). Daily mean relative humidity seldomly drops below 50% in summer when free atmosphere air is cooled near the cold glacier surface, increasing relative humidity. Periods with drier air occur from October to May and are most frequent from February to April. The seasonal cycle of specific humidity follows air temperature (Figure 5). In summer, specific humidity is comparable under clear and overcast skies, while in winter, overcast skies are associated with more humid conditions.

5.3. Wind Speed and Wind Direction

[27] Daily mean wind speeds higher than 10 m s^{-1} are not exceptional on Midtdalsbreen (Figure 3). In autumn and winter, when storms frequently come in from the Atlantic Ocean, wind speeds are considerably larger than in summer. Compared to the other five winters, the winter 2004–2005 was exceptionally windy, with monthly mean wind speeds of 10.4 m s^{-1} in December 2004 and 10.0 m s^{-1} in January 2005. Daily mean wind speeds are less variable in the summer season and are typically 5–6 m s^{-1}. Throughout the year, wind speeds are highest under overcast conditions (Figure 5).

[28] Figure 6 shows the distribution of wind directions for clear-sky and overcast conditions. Remarkable differences can be seen between the two panels. Under overcast skies, westerly and south-easterly winds prevail. These wind directions are also the single two wind directions observed at the NMI automatic weather station Finsevatn (1210 m a.s.l., F in Figure 1). Finsevatn is located in the middle of the valley Finsedalen, Midtdalsbreen is situated on the southern valley wall. Finsedalen has a west–east orientation west of Finsevatn, changing to a northwest–southeast orientation east of Finsevatn. The topography likely channels the large-scale winds, resulting in either westerly or south-easterly wind directions. Westerly winds are most common, especially for higher wind speeds. A third dominant wind direction is found for clear-sky conditions and wind speeds below 5 m s^{-1}, blowing down-slope along the glacier's length axis. This glacier wind, or katabatic wind, is induced by the turbulent cooling of air above the colder glacier surface.

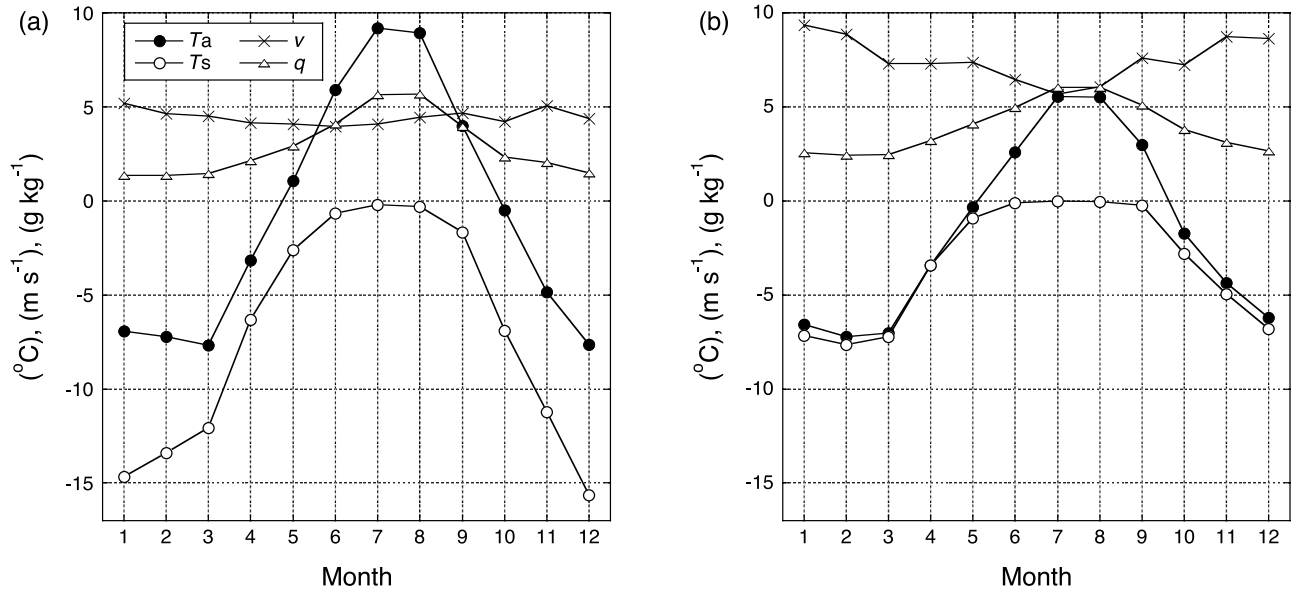

Figure 5. Monthly average values of air and surface temperature (T_a and T_s in °C), wind speed (v in m s^{-1}), and specific humidity (q in g kg^{-1}) for (a) clear-sky and (b) overcast conditions. T_s calculated with the energy balance model is shown here.

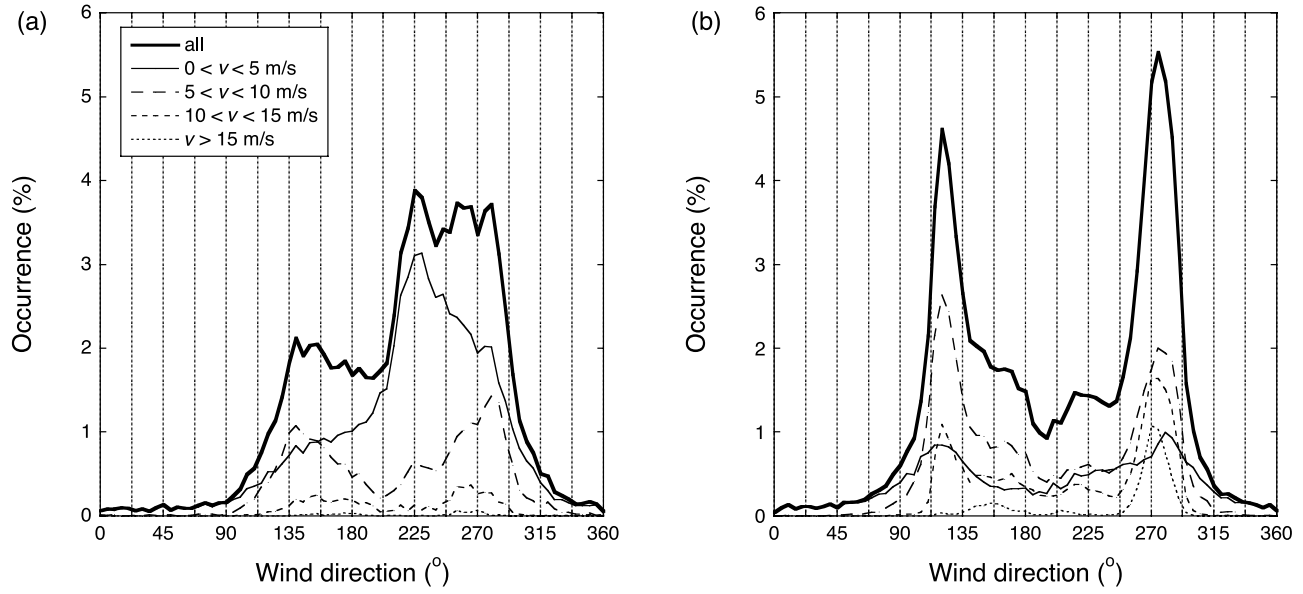

Figure 6. Distribution of wind direction for (a) clear-sky and (b) overcast conditions. The overall curve is shown together with a subdivision into wind speed intervals.

5.4. Surface Height

[29] Daily mean values of the surface height at the AWS site are shown in Figure 7. By showing the period 1 October to 30 September, approximately one accumulation and one ablation season are captured for each individual year. In three of the six years, some ice melted in October before the snowpack started to build up. With almost no melt episodes in winter and an occasional snowfall event during summer, every year can nearly be separated into a pure accumulation and ablation phase. The months April, May, September, and October are transitional months between the two phases, when both snowfall and melt occur. The timing and amount of solid precipitation in winter differs greatly from year to year. The maximum snow depth, a little over 3 m, was recorded in April 2005. The surface became snow-free at dates between 10 June (in 2002) and 17 July (in 2005). Figure 7 illustrates that the large variability in the date of snow disappearance is primarily related to the amount of snow received in winter, the meteorological conditions in spring are of secondary importance. The total amount of ice melted in a year has a wide range, from 3 m in 2001 and 2005 to almost 6 m in 2002.

6. Surface Energy Fluxes

6.1. Seasonal Cycle

[30] Figure 8 shows the seasonal cycle of the surface energy balance for clear-sky and overcast conditions. S_{net} increases steadily from January to its maximum in July, a combined effect of increasing top of the atmosphere irradiation and a decreasing snow albedo. The maximum is not found at the summer solstice in June, as the ice surface with a significantly lower albedo than snow does not appear before July in most years. S_{net} decreases rapidly after August; snowfall events in September and October increase the surface albedo. L_{net} is maximum in July and August, when temperatures are highest. Under overcast skies, L_{net} is positive in summer and slightly negative during the rest of the year. For clear-sky conditions, L_{net} is always negative. The turbulent fluxes have a maximum in summer, when the surface temperature is limited to the melting point and the temperature difference between the air and the surface is large. For clear-sky conditions, H_{sen} has a second maximum in winter. The reason is that in summer, S_{net} compensates for the negative L_{net}, while in winter S_{net} is small and H_{sen} and G transport heat toward the cooling surface. H_{lat} is always larger for overcast conditions than under clear skies, be-

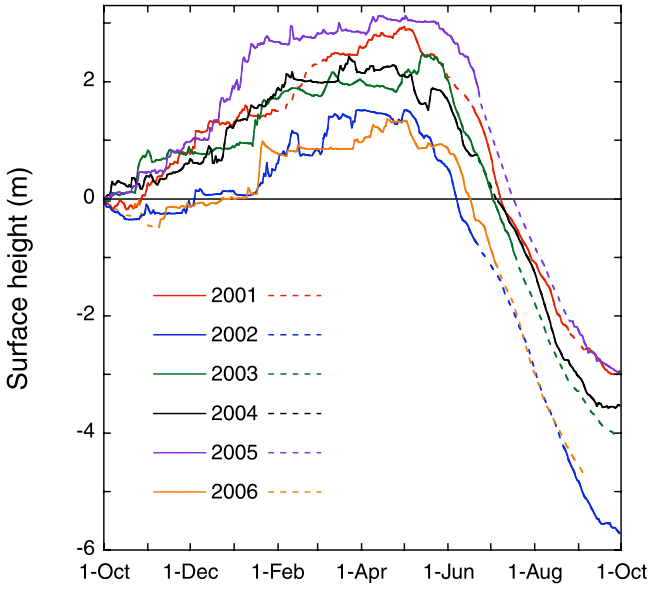

Figure 7. Daily mean surface height for the entire record, divided into periods from 1 October (previous year) to 30 September. Solid lines are measurements by the sonic ranger, the dashed lines are reconstructed accumulation (from precipitation measured at precipitation station Liset) and melt (calculated with the energy balance model).

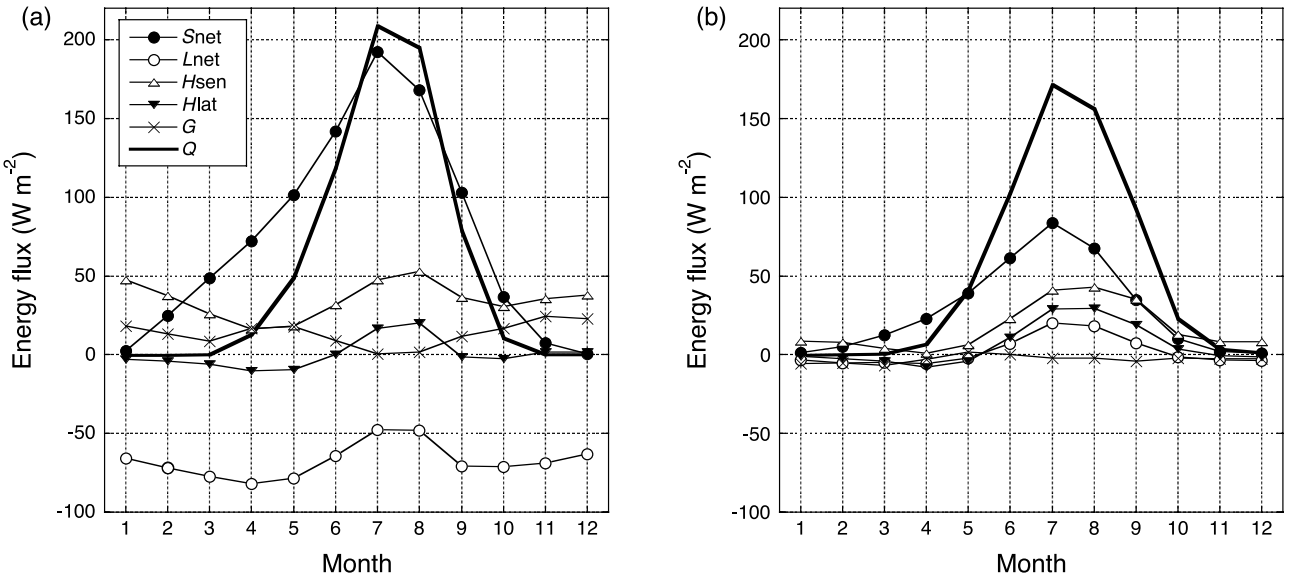

Figure 8. Monthly average values of the surface energy fluxes for (a) clear-sky and (b) overcast conditions.

cause of more humid and windier conditions associated with cloudy skies (Figure 5). The main melt season is from May to October. Although all fluxes are positive or near zero under overcast skies, the energy available for melt is generally higher for clear-sky conditions. This can be attributed to the large difference in S_{net} between clear-sky and overcast conditions. From May to September, the difference in S_{net} between clear and overcast skies is larger than the difference in L_{net}. A contrasting situation applies during the remainder of the year when, because of a high surface albedo, the reduction in S_{net} for cloudy compared to clear-sky conditions is smaller than the gain in L_{net}; an example of the albedo paradox [*Ambach*, 1974].

6.2. Interannual Variability

[31] The glacier surface is melting ($Q > 0$) for 33 to 37% of the year, with an average melt energy of 151 W m^{-2} (Table 3). The sum of all half-hourly periods with melt (Σt_{melt}) was largest in 2002 and smallest in 2003. S_{in} is the major source of energy for surface melt, while L_{out} is the major energy sink. H_{sen} supplies more than twice as much energy as H_{lat}, this is mainly because H_{lat} is often negative in spring. The subsurface heat flux is small compared to the other fluxes. Comparison of the average energy fluxes during melt in different years is complicated by the fact that the numbers depend on the distribution of the half-hourly periods with melt over the melt season. For example, in 2003 the mean melt energy was much larger than in 2005, but the amount of melt is very similar, because the sum of all melt periods is smaller for 2003. To facilitate the comparison of the energy fluxes for different years, we normalized the mean fluxes by multiplying each flux by Σt_{melt} for that year and dividing by the average Σt_{melt} over all the years. These normalized fluxes show that surface melt was largest in 2002 and smallest in 2001 (Figure 9). This was already shown in Figure 7 for ice melt; in Figure 9 snow melt is also included. Because of less winter accumulation on Midtdalsbreen in 2002, the snow disappeared early this year. The lower ice albedo increased S_{net}, while high air temperatures resulted in larger turbulent fluxes. In 2001, the low melt rate was a combined result of relatively low S_{in}, as well as low air temperatures and wind speeds.

[32] The interannual variability in the melt energy is determined by a combination of variations in S_{net} and variations in the turbulent fluxes, which have comparable magnitudes. The variability in S_{net} again depends on variations in both S_{in} and S_{out}, while interannual variations in the turbulent fluxes are determined by variability in both air temperatures and wind speeds. L_{in}, and hence L_{net}, show little variation over the five melt periods. As L_{in} increases with increasing air temperatures and cloudiness, and high air temperatures in summer are often associated with clear skies and vice versa, the variability in L_{in} is reduced.

6.3. Relative Contribution to the Melt Energy

[33] Net solar radiation contributes on average 75% of the melt energy, the turbulent fluxes together account for 35%, while net longwave radiation and the subsurface heat flux are energy sinks of 8% and 2%, respectively (Table 4). The percentage of the total melt energy supplied by net solar radiation was largest in 2004 and smallest in 2005. In 2004, sunny conditions persisted for more than a week around the

Table 3. Sum of All Half-Hourly Periods with Melt Σt_{melt} (days) and Mean Values of the Surface Energy Fluxes (W m^{-2}) for the Periods With Melt in Each Individual Year

	2001	2002	2003	2004	2005	Mean
Σt_{melt}	130	137	121	122	136	129
Q	133	165	162	150	144	151
S_{in}	236	244	242	257	234	242
S_{out}	−132	−122	−125	−139	−130	−129
L_{in}	304	303	304	303	304	304
L_{out}	−316	−316	−316	−316	−316	−316
H_{sen}	31	41	40	34	38	37
H_{lat}	13	17	18	12	18	15
G	−2	−2	−2	−2	−3	−2

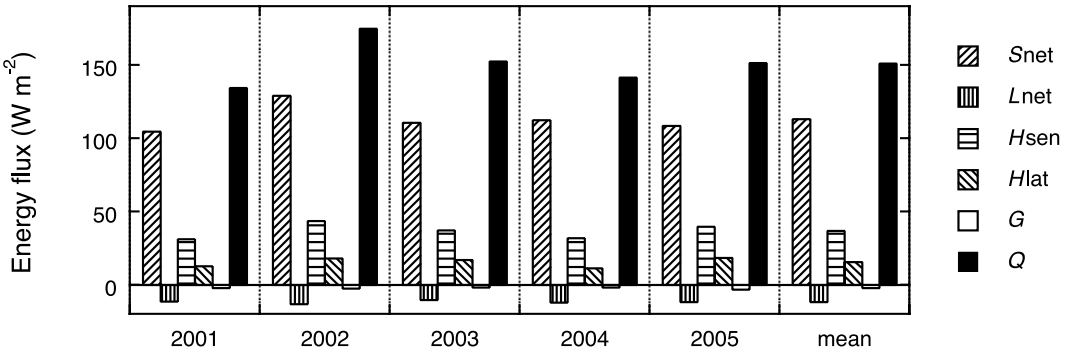

Figure 9. Normalized average surface energy fluxes for the periods with melt in each individual year. For normalization, the mean of all half-hourly values with melt in a particular year was multiplied by the sum of all periods with melt in that year and divided by the average sum of periods with melt over all years.

end of May, the period with almost the maximum amount of S_{in}, resulting in above-average values for S_{net}. On the other hand, below or around average air temperatures, humidity and wind speeds lead to relatively small turbulent fluxes. In 2005, total accumulation was high and the snowpack disappeared later than in the other years. Combined with relatively low S_{in} due to cloudy weather, S_{net} was smaller than on average, while high wind speeds lead to above-average turbulent fluxes. Compared to the other fluxes, the contribution by L_{net} is very similar for the different years.

[34] Many glacio-meteorological studies report the relative contributions of net (shortwave and longwave) radiation and turbulent fluxes to surface melt. At the AWS site on Midtdalsbreen, net radiation supplies on average 67% of the melt energy, while the turbulent fluxes account for 35%, the subsurface heat flux is a small energy sink of 2%. Our value for the contribution of net radiation lies in between average values for continental glaciers (77%) and maritime glaciers (50%) reported by *Willis et al.* [2002]. It is comparable to values on Peyto Glacier, Canada (65%) [*Munro*, 1990] and on Storglaciären, Sweden (66%) [*Hock and Holmgren*, 1996].

[35] Looking at clear-sky conditions only, the contribution of S_{net} to surface melt is about 35% larger than for all-sky conditions (Table 4). Under clear skies, L_{net} is a large energy sink which cannot be compensated for by the turbulent fluxes alone, hence the contribution by S_{net} is larger than 100%. In 2001 and 2002 the contribution of S_{net} to melt under clear skies deviated largely from the average over the total period. In 2001, almost all clear-sky periods with melt occurred in spring, when the relative contribution of the turbulent fluxes to melt is small. On the other hand, August 2002 was unusually sunny, but in this month the relative importance of the turbulent fluxes is larger than in spring, resulting in a lower contribution by S_{net}. For overcast conditions, S_{net} is less dominant and contributes on average only slightly more to surface melt than the turbulent fluxes. The contribution by L_{net} is positive under overcast skies. For clear-sky days, S_{net} and L_{net} together are approximately 10% more important for melt than on average, while their contribution is 10% smaller for overcast skies. These differences between clear and overcast skies are almost entirely resulting from the large absolute differences in S_{net} and L_{net}; the average values for the turbulent fluxes are comparable. However, on overcast days, H_{lat} supplies a larger part of the total energy from the turbulent fluxes than on clear-sky days, because the air is more humid. Averaged over the five complete years, net radiation during melt is a factor of two larger for clear skies compared to overcast skies. Even though the melt rate is considerably larger for clear-sky conditions, almost 60% of the total ablation occurs under cloudy conditions, where cloudy is defined as $n > 0.5$. This percentage ranges from 55% in 2002 to 71% in 2005.

7. Discussion

7.1. Model Sensitivity to Variations in z_{0v} and the Stability Correction

[36] The turbulent fluxes play a significant role in the surface energy balance, but also have a large uncertainty, as they need to be calculated from other quantities. In literature, many different methods have been employed to calculate the turbulent fluxes, mainly depending on the

Table 4. The Contribution of the Surface Energy Fluxes to Surface Melt (%) for All-Sky, Clear-Sky and Overcast Conditions for the Periods With Melt in Each Individual Year[a]

	2001	2002	2003	2004	2005	mean
All-sky						
S_{net}	78	74	73	79	72	75
L_{net}	−9	−8	−7	−9	−8	−8
H_{sen}	23	25	24	23	26	24
H_{lat}	9	10	11	8	12	10
G	−2	−1	−1	−1	−2	−2
Clear-sky						
S_{net}	127	98	106	106	121	109
L_{net}	−40	−30	−27	−30	−41	−32
H_{sen}	15	27	20	22	22	21
H_{lat}	0	6	4	2	1	3
G	−1	−1	−2	−1	−3	−2
Overcast						
S_{net}	50	50	43	52	47	48
L_{net}	10	11	10	9	8	10
H_{sen}	28	26	29	26	29	28
H_{lat}	15	15	18	14	18	16
G	−2	−2	−1	−1	−2	−2

[a]Percentages have been rounded to the nearest integer, therefore their sum is not always exactly 100%.

measurements available. As stable stratification is common over melting glaciers, turbulence is expected to be reduced and stability corrections should be applied. However, *Konzelmann and Braithwaite* [1995] and *Hock and Holmgren* [1996] found that the measured surface melt was underestimated when stability corrections were included in the calculation of the turbulent fluxes. For this and other reasons, stability corrections have been neglected in several energy balance studies on glaciers [*Hock and Holmgren*, 1996; *Oerlemans and Klok*, 2002; *Konya et al.*, 2004]. Another uncertainty is associated with the specification of roughness lengths, as these are both temporally and spatially highly variable [*Brock et al.*, 2006]. Often, the available measurements are not sufficient to determine estimates of the roughness lengths. In several studies, values for the roughness lengths are therefore taken from published studies [e.g., *Klok et al.*, 2005; *Arnold et al.*, 2006] or used as tuning parameters to match measured melt or sublimation [*Wagnon et al.*, 1999; *Oerlemans and Klok*, 2002; *Hock and Holmgren*, 2005]. Previous studies showed that when the roughness lengths for momentum, heat and moisture are assumed to be the same, an order-of-magnitude increase in these roughness lengths leads to a doubling of the turbulent fluxes [*Munro*, 1989; *Braithwaite*, 1995]. Similarly, in a study where only z_{0v} was increased by an order of magnitude, a 25% error in the turbulent fluxes was reported [*Denby and Greuell*, 2000]. *Munro* [1989] noticed that this error becomes smaller when z_{0T} is not prescribed, but calculated following *Andreas* [1987]. In Andreas' model, an increase in z_{0v} results in a decrease in z_{0T}, which partly compensates for the change in z_{0v}. *Klok et al.* [2005] applied this model and found an increase in the turbulent fluxes of 19% for a tenfold increase in z_{0v}, while omitting the stability functions lead to a much larger increase (43%). Our energy balance model is similar to their model, the main difference is that in our model T_s is calculated and not taken from measurements. In line with these previous studies, we determined the sensitivity of our energy balance model to the value of z_{0v} and the stability correction applied.

[37] The values for z_{0v} for ice and snow were varied separately by two orders of magnitude within the ranges most commonly observed on glaciers [*Brock et al.*, 2006]. The roughness length is expected to fluctuate within this range. Hence the runs with very high and low values of z_{0v} give extreme values that will not likely be attained. We determined the effect of a varying z_{0v} by using one single value for z_{0v} for snow and ice surfaces, so $z_{0v,i} = z_{0v,s} = z_{0v}$. We report the sensitivity with respect to the reference value $z_{0v} = 1$ mm instead of values used in this study, to provide more general results for comparison with other models. The effect of a separate roughness length for snow was investigated by keeping $z_{0v,i}$ constant at the reference value while $z_{0v,s}$ was varied. The entire measurement period was included in the calculations; results are listed in Table 5. Model results for the z_{0v} values used in this study are also reported to allow for a comparison with the reference value.

[38] Taking $z_{0v} = 1$ mm as the reference case, we see that an increase (decrease) in z_{0v} of one order of magnitude results in a 11% increase (16% decrease) in the mean turbulent fluxes and an increased (decreased) ice melt of 5% (7%). Using a separate value for z_{0v} over snow has little effect on the surface melt, since the majority of the melt occurs when the surface is ice. Variation of z_{0v} has more impact on the turbulent fluxes for ice surfaces, while over snow the variation in ΔT_s is larger between the different runs. These results can be explained by the model design. Given a value for z_{0v}, the model determines in every timestep the set of values for T_s, z_{0T}, z_{0q} and L_{MO} which, by the associated values for L_{out}, G and the turbulent fluxes, results in a closure of the energy balance. When the optimal value for T_s is higher than the melting point temperature, T_s is set back to 0°C and the excess energy is used for melting. For a melting surface, L_{out} and G have determined values and only the turbulent fluxes and the melt energy are variable. The ice surface is often at the melting point temperature while the temperature of the snow surface can generally vary over a wider range. Hence changing z_{0v} for an ice surface mainly affects the turbulent fluxes and the melt energy, for a snow surface L_{out} and G will also change and the relative change in the turbulent fluxes and the melt energy will be smaller. The model used here is less sensitive to the choice of z_{0v} than models used in several other studies [*Braithwaite*, 1995; *Hock and Holmgren*, 1996; *Brock et al.*, 2006], because a change in z_{0v} does not directly lead to a change in turbulent fluxes and melt, but to a different solution of the energy balance which generally damps the effect. By solving the energy balance, the effect of small errors in measurements and model parameters is reduced and the time evolution of the surface energy fluxes is consistent. However, when the errors are larger because of measurement problems or an incorrect representation of the surface energy balance, the model may still be able to obtain values for the energy fluxes, but the residual in the energy balance will be larger and ΔT_s will increase.

[39] In this study we use separate, but constant values for $z_{0v,i}$ and $z_{0v,s}$. In reality, these values will vary on hourly to seasonal time scales. Assuming that values for z_{0v} fluctuate within the ranges presented in Table 5, the errors in individual values of the turbulent fluxes are estimated to be 20%. The numbers reported in Tables 3 and 4 represent melting conditions, when the sensitivity of the turbulent fluxes to z_{0v} is largest. Recalculating the numbers in Table 3 using $z_{0v} = z_{0v} = 5$ mm, which we regard as an upper limit for z_{0v} on Midtdalsbreen, the mean value of the turbulent fluxes increases by 9 W m^{-2} (18%). A 9 W m^{-2} increase in the turbulent fluxes is also found for clear-sky and overcast conditions separately, with the difference that H_{sen} is mainly affected for clear skies (+8 W m^{-2}), while for overcast skies the increase in H_{sen} is only 2 W m^{-2} larger than the increase in H_{lat}. The larger turbulent fluxes result in a 4% increase in their contribution to melt (Table 4), a similar decrease in the contribution by S_{net} and less than 1% change in the other fluxes. These numbers also apply to clear-sky and overcast conditions separately, although for clear skies the contribution by H_{sen} changes by 4%, for overcast skies the contributions by H_{sen} and H_{lat} both change by 2%.

[40] Furthermore, we investigated the effect of the stability correction by running the model without applying a stability correction and with the full (not limited) stability correction. The results reveal that neglecting atmospheric stability corrections or using the full stability correction for stable cases, has a larger impact on the turbulent fluxes and surface melt than an order-of-magnitude change in the value of z_{0v} (Table 5). This is contrary to the findings of

Table 5. Sensitivity of the Mean Turbulent Fluxes Δ ($H_{sen} + H_{lat}$), Total Surface Melt ΔM and Modeled Surface Temperature (Expressed as the Mean Deviation ΔT_s From the Observed Surface Temperature) to the Values of $z_{0v,i}$, $z_{0v,s}$ and Stability Corrections[a]

z_{0v} (mm)		Δ (H_{sen}+ H_{lat}) (%)			ΔM (%)			ΔT_s (°C)		
Ice	Snow	All	Ice	Snow	All	Ice	Snow	All	Ice	Snow
0.1	0.1	−15.7	−19.0	−11.4	−7.1	−7.8	−5.5	−0.00	−0.13	+0.05
0.5	0.5	−4.1	−4.9	−2.9	−1.9	−2.0	−1.5	+0.09	−0.11	+0.16
1.0	1.0	0.0	0.0	0.0	0.0	0.0	0.0	+0.11	−0.10	+0.19
5.0	5.0	+7.9	+9.7	+5.6	+3.7	+4.0	+3.1	+0.16	−0.09	+0.26
10.0	10.0	+11.2	+13.8	+7.9	+5.3	+5.7	+4.3	+0.18	−0.08	+0.28
1.0	0.01	−10.2	0.0	−23.3	−3.0	0.0	−10.5	−0.13	−0.10	−0.15
1.0	0.05	−6.6	0.0	−15.0	−2.1	0.0	−7.3	−0.03	−0.10	−0.01
1.0	0.1	−4.9	0.0	−11.2	−1.6	0.0	−5.5	+0.01	−0.10	+0.05
1.0	0.5	−1.3	0.0	−2.9	−0.4	0.0	−1.5	+0.11	−0.10	+0.16
0.75	0.13	−5.4	−2.0	−9.7	−2.0	−0.8	−4.8	+0.02	−0.10	+0.07
No Stability Correction										
1.0	1.0	+20.6	+26.1	+13.6	+9.7	+10.7	+7.1	+0.26	−0.06	+0.38
0.75	0.13	+21.9	+26.7	+15.1	+9.9	+10.8	+7.3	+0.18	−0.06	+0.27
Full Stability Correction										
1.0	1.0	−14.4	−16.4	−11.8	−5.5	−6.5	−3.0	−0.14	−0.18	−0.12
0.75	0.13	−15.8	−17.2	−13.7	−5.8	−6.8	−3.3	−0.24	−0.18	−0.27

[a]Except for ΔT_s, relative changes are given with respect to the reference value $z_{0v,i} = z_{0v,s} = 1.0$ mm. Average values have been determined over the entire period (all), periods with an ice surface (ice) and periods with snow cover (snow).

Braithwaite [1995] who found a larger effect for changes is z_{0v}. In that study, equal values were chosen for the roughness lengths of momentum and heat, which explains the large sensitivity to a change in z_{0v}. The values found here for ice surfaces are of the same magnitude as the values found by *Klok et al.* [2005], which is not surprising considering the similarity of the models used. Omitting the stability corrections does not significantly deteriorate the model performance, although the overall value for ΔT_s is larger. On the other hand, using the full stability correction leads to a systematic underestimation of T_s and a larger RMSE (1.5°C, not shown).

[41] From these results, it is difficult to say whether applying a stability correction is necessary. If the correction is omitted, the amount of ice melt increases by 10%, lessening the agreement with the melt measured at the ablation stakes. Omitting the stability correction for overcast conditions induces changes in the turbulent fluxes during melt comparable to changing z_{0v} to 5 mm. For clear-sky conditions the effect on the turbulent fluxes is larger (+17 W m^{-2}), as the air is generally stably stratified under clear skies. Applying the full stability correction hardly changes the fluxes under overcast skies, for clear-sky conditions the turbulent fluxes decrease by 14 W m^{-2}. For clear-skies, the contribution of the turbulent fluxes to melt (Table 4) increases (decreases) by 8% (7%) when the stability correction is omitted (not limited). For overcast skies, the respective contributions only change by +4% and −2%. Interestingly, changing z_{0v} or the stability correction significantly affects the values reported for the turbulent fluxes in Tables 3 and 4, but the absolute value of L_{in} (and hence L_{net}) does not change by more than 1 W m^{-2} and the contribution to melt varies less than 1% for all cloud conditions.

[42] The results indicate that one should be careful with stability corrections when the turbulent fluxes are calculated from measurements made at a level above the wind speed maximum. We can conclude that when using this type of model, the errors introduced by the uncertainty in the turbulent fluxes are of the same order of magnitude as uncertainties in the radiation measurements and other model parameters, for example the value assumed for the ice density. Therefore, when attempting to further improve the model, all these factors need to be addressed.

7.2. Interannual Variability in the Total Melt

[43] The interannual variability in the total melt is a combined result of changes in surface properties, which are largest at the moment the snow cover disappears, and variations in meteorological conditions. To estimate the separate effects of these two processes on the total annual melt, we performed additional model runs with prescribed albedo and snow depth series. When snow is present, the snow depth is set to 1 m. On a given date, snow depth is set to zero and the albedo is switched from snow to ice albedo. Hence the moment of ice appearance is controlled and not determined by the meteorological conditions. To remove the effect of small variations in albedo that could complicate the comparison, we used two constant albedo values representing snow and ice conditions. Together with measured S_{in}, these values prescribe S_{net} in the model. Albedo values of 0.70 for melting snow and 0.31 for ice produce annual melt values less than 0.2 m w.e. larger than the melt calculated with the measured albedo series, except in 2002 where the melt is overestimated by 0.4 m w.e. The differences originate when a constant albedo is not a good approximation, for example during summer snowfall events. Nevertheless, the resemblance is good enough for this analysis.

[44] The model was run with five different albedo series: always ice (albedo = 0.31), always snow (albedo = 0.70), snow disappears on 11 June as in 2002 (the earliest date), snow disappears on 18 July as in 2005 (the latest date) and snow disappears on the observed date. The modeled melt for these five runs is shown in Figure 10. Melt is defined as the amount of water produced at the surface, still including the water that later possibly refreezes in the snowpack. For the hypothetical all-year ice surface, total

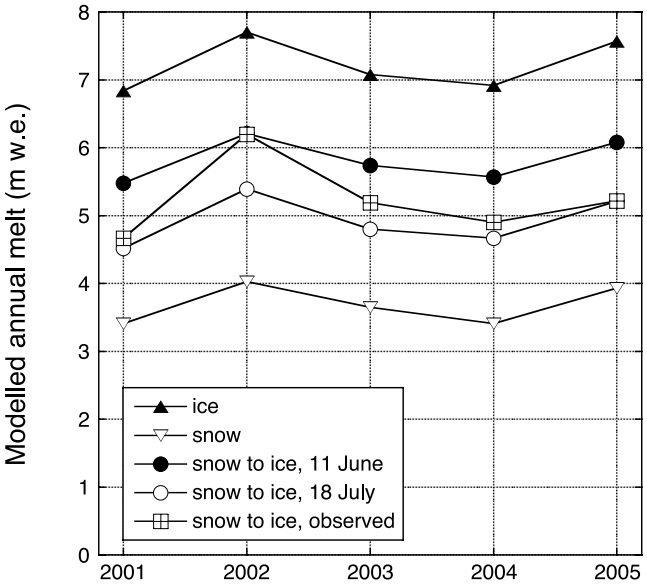

Figure 10. Modelled annual melt for five albedo series, where the snow albedo is 0.70 and the ice albedo 0.31. The labels refer to runs with always ice, always snow, snow disappearance on 11 June, snow disappearance on 18 July, and snow disappearance on the observed date.

melt is almost twice as large as for an all-year snow cover. This result demonstrates the dominating influence of the albedo on melt. In May and June, melt is most sensitive to albedo changes, in both months melt increases by approximately 0.8 m w.e. when the surface is ice instead of snow (not shown). Varying the date of snow disappearance by 37 days according to the spread in the observations induces a mean change in melt of 0.9 m w.e. with little variability between the years. The four simulations with identical albedo series for all years demonstrate the influence of the meteorological conditions during the melt season on interannual variability, amounting to a maximum difference in melt between 2001 and 2002 of 0.8 m w.e. We see that even when the albedo effect of the thin snowpack is removed, 2002 still has the largest amount of melt, a result of the high summer temperatures (Figure 3). The simulations also show that the melt in 2002 and 2005 would have been comparable when the snow cover had disappeared around the same time, provided that the meteorological conditions for the data gap in 2005 have been simulated adequately. Even with the albedo effect removed, 2001 remains the year with the minimum total melt. We can conclude that for these five years, the interannual variability in total melt induced by meteorological conditions during the melt season is of the same magnitude as the albedo effect of an early or late disappearance of the snowpack. Under identical meteorological conditions, the date of ice appearance depends solely on the total winter accumulation. The experiment shows that variations in winter mass balance at the AWS location not only affect the net mass balance directly, but also have a significant effect on the total melt, and hence net mass balance, via a positive albedo feedback mechanism. Unfortunately, this finding cannot simply be generalized to other years or other locations, which may have different variability in snow accumulation and meteorological conditions.

7.3. Comparison With Morteratschgletscher

[45] In this section, we compare the seasonal cycles of meteorological variables and surface energy fluxes on Midtdalsbreen with measurements from an IMAU–AWS (2100 m a.s.l.) on Morteratschgletscher, Switzerland [*Oerlemans and Klok*, 2002]. This comparison of two isolated records from two different regions should not be regarded as a comparison of the climates in the European Alps and Norway. Irrespective of the question of representability, the two glaciers differ in many aspects: Morteratschgletscher is situated at a lower latitude, in a drier environment and is surrounded by higher mountains than Midtdalsbreen. The comparison of two long AWS records from these locations gives insight in differences in meteorological variables and the surface energy balance originating from the characteristics of the glaciers and their environment.

[46] The two AWSs have a similar design, except that on Morteratschgletscher the measurement level is at 3.5 m above the ice surface. This data set spans the period 8 July 1998 to 14 May 2007. We selected a subset of the data corresponding to the period used for Midtdalsbreen (2 October 2000 to 7 September 2006) and applied the same energy balance model (section 4.1) to the data. Only the initial subsurface temperature profile and the snow density (300 kg m^{-3}) were changed. The method to derive cloudiness described in section 3.4 did not give robust results for Morteratschgletscher, cloud fractions tended to be overestimated in summer because of higher minimum values for L_{in} in this season. Although a detailed cloud analysis could not be done in this case, the mean cloud fraction calculated for Morteratschgletscher (0.47) is considerably lower than on Midtdalsbreen (0.61, Table 2). At the AWS site on Morteratschgletscher the maximum snow depth ranges between 0.3 and 2 m, the surface already becomes snow-free in May. During the period considered here, the measured ice ablation amounts to 40.8 m, almost twice as much as on Midtdalsbreen (24.0 m).

[47] The seasonal cycles of meteorological variables on the two glaciers (Figures 11a and 11b) show clear differences. Throughout the year, air temperatures are higher at the AWS site on Morteratschgletscher, despite the 650 m higher altitude of this station. The temperature difference is largest in spring and autumn, probably because the seasonal cycle in solar irradiance is larger on Midtdalsbreen and the snow cover disappears later. In winter, surface temperatures are much lower on Morteratschgletscher because of more frequent clear-sky conditions, values are more comparable to surface temperatures on Midtdalsbreen under clear skies (Figure 5a). Wind speeds are higher on Midtdalsbreen, especially in winter. The wind climate on Midtdalsbreen is dominated by the large-scale circulation (section 5.3), while katabatic winds prevail on Morteratschgletscher [*Oerlemans and Grisogono*, 2002]. The absolute values and the seasonal cycles of specific humidity are very similar on the two glaciers, although relative humidity values are much lower on Morteratschgletscher (annual mean 64.9%). Hence climatic conditions on Midtdalsbreen are generally colder, cloudier, more humid and windier than on Morteratschgletscher.

[48] The seasonal cycles of the surface energy fluxes (Figures 11c and 11d) show that the melt season starts

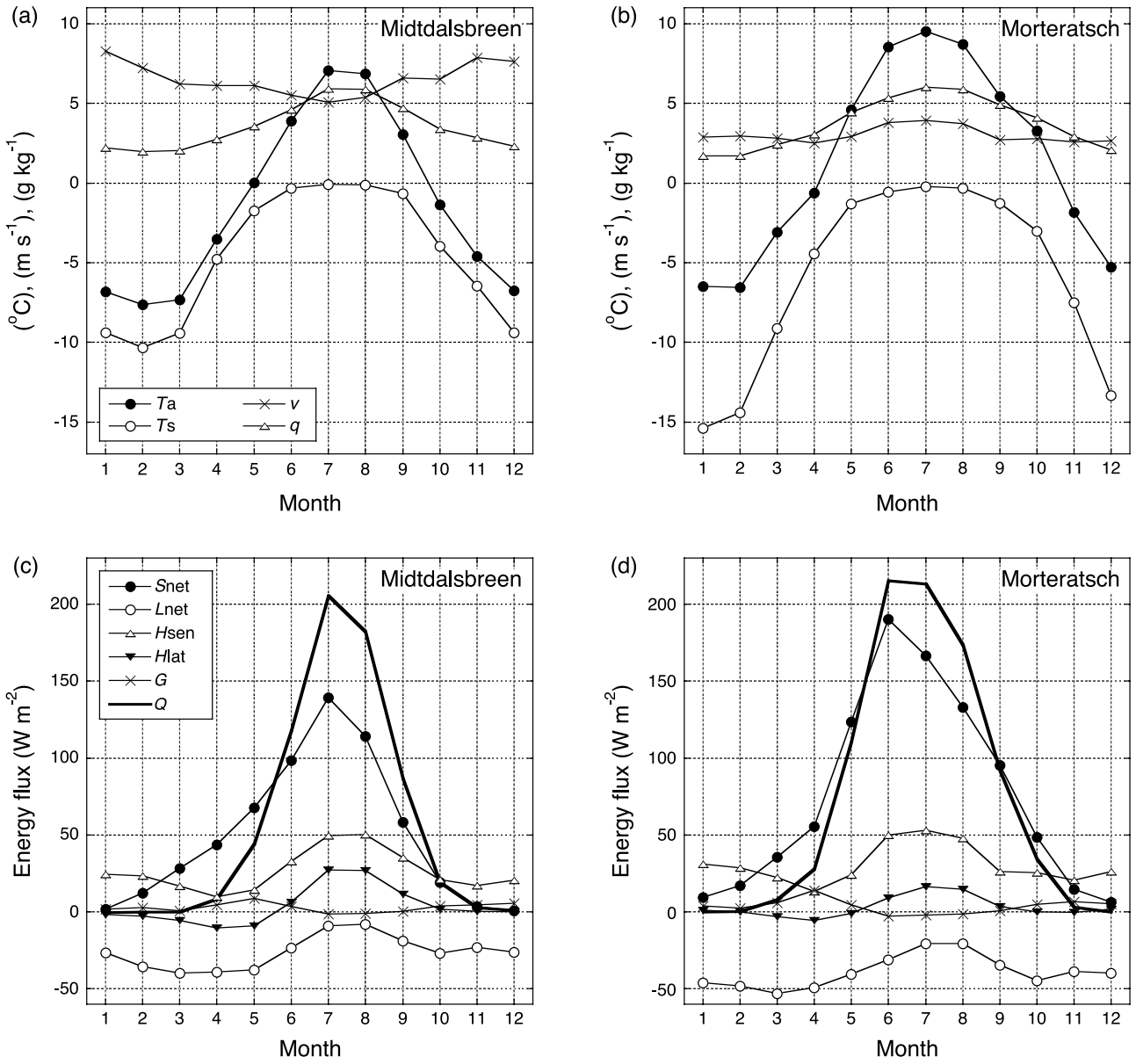

Figure 11. Monthly average values of air and surface temperature (T_a and T_s in °C), wind speed (v in m s^{-1}) and specific humidity (q in g kg^{-1}) for (a) Midtdalsbreen and (b) Morteratschgletscher. T_s calculated with the energy balance model is shown here. Monthly average values of the surface energy fluxes for (c) Midtdalsbreen and (d) Morteratschgletscher.

earlier on Morteratschgletscher. The melt energy already reaches a maximum in June, while on Midtdalsbreen the melt energy is maximum in July. From July to September, absolute values for the melt energy are comparable at the two AWS locations. However, the relative contribution of the surface energy fluxes to the melt energy is different for the two glaciers. S_{net} is larger and more dominant on Morteratschgletscher because of an earlier disappearance of the snowpack and a lower ice albedo. From May to July, S_{in} is larger on Midtdalsbreen, even though the incoming solar radiation at the top of the atmosphere is smaller and the cloud fraction is larger. At the AWS location on Morteratschgletscher, S_{in} is significantly reduced because of shading by the surrounding topography [*Klok and Oerlemans*, 2002], but multiple reflection of solar radiation by the snow cover may also contribute to a higher S_{in} on Midtdalsbreen. Despite the lower air temperatures, L_{net} is more positive on Midtdalsbreen throughout the year; a result of the frequent clouds on Midtdalsbreen which increase L_{in}. The seasonal cycle of H_{sen} is comparable at the two locations; the effect of lower air temperatures on Midtdalsbreen is compensated by the higher wind speeds. In June, H_{sen} is considerably larger on Morteratschgletscher due to the higher air temperatures. H_{lat} is more negative in spring and more positive in summer on Midtdalsbreen. As the annual cycle in specific humidity is comparable at the two locations, this is also a result of the windier conditions on Midtdalsbreen.

[49] The number of half-hourly periods with melt is similar at the two AWS sites (35% of the year for Midt-

dalsbreen and 36% for Morteratschgletscher), but the mean melt energy during these periods is 36% larger on Morteratschgletscher (202 W m^{-2}). The mean value of S_{net} during melt is 68 W m^{-2} (60%) larger on Morteratschgletscher and contributes on average 90% of the melt energy. The differences between the other fluxes are smaller; mean values for L_{net} and H_{lat} during melt are 11 W m^{-2} and 7 W m^{-2} smaller than on Midtdalsbreen, H_{sen} is 5 W m^{-2} larger. Hence the larger ablation on Morteratschgletscher primarily results from an earlier start of the melt season, a thinner snowpack and a lower ice albedo.

8. Conclusions

[50] We analyzed a 6-year meteorological record from Midtdalsbreen to determine the seasonal and interannual variation of meteorological quantities and the surface energy and mass balance. Subsets for clear-sky and overcast conditions were created to study the effect of clouds on the surface energy balance. Cloudy conditions are found to prevail in all seasons with generally higher wind speeds and humidity values than during clear-sky conditions.

[51] Because of the pronounced annual cycle of incoming solar radiation at the glacier's latitude, the surface energy balance shows a large seasonal cycle. Between September and May, net radiation under overcast skies is larger than for clear-sky conditions. From the beginning of May until the end of September, surface melt is likely to occur. The winter snowpack disappears around the beginning of July, the exact timing varies by more than a month and is related to the maximum snow depth. The annual ice ablation ranges from 3 m in 2001 and 2005 to almost 6 m in 2002. Surface melt is dominated by net solar radiation. On average, it contributes 75% of the total melt energy, net longwave radiation contributes negatively (−8%). The remaining 33% is accounted for by the turbulent fluxes (35%) and the subsurface heat flux (−2%). For clear-sky conditions, the contribution by net radiation is approximately 10% larger, while for overcast skies, net radiation is about 10% less important than on average. The average melt rate is larger under clear skies, but because of the frequent occurrence of cloudy conditions, almost 60% of the melt occurs under cloudy skies. The albedo effect induced by variable snow disappearance dates affects the interannual variability by the same magnitude as varying meteorological conditions during the melt season. Varying meteorological conditions mainly have an effect on net solar radiation and the turbulent fluxes; net longwave radiation shows little variability. In winter, all energy fluxes are close to zero for overcast conditions, while for clear skies the negative net longwave radiation is balanced by the sensible heat flux and the subsurface heat flux.

[52] The results for Midtdalsbreen were compared with measurements from an AWS on Morteratschgletscher, Switzerland. Climatic conditions on Midtdalsbreen are generally colder, cloudier, more humid and windier than on Morteratschgletscher. The earlier start of the melt season, the thinner snowpack and the lower ice albedo on Morteratschgletscher result in almost twice as much ice ablation as on Midtdalsbreen, primarily a result of larger net solar radiation.

[53] The energy balance model was found to be more sensitive to the way stability corrections are applied than to an order-of-magnitude change in the surface roughness length for momentum. Compared to other studies, the model we use is less sensitive to the value of the surface roughness length for momentum. This is because of the model design, the model closes the energy balance by varying the surface temperature and the roughness lengths for heat and moisture. In this way, small errors in the model parameters and the measurements will not result in very different solutions for the turbulent fluxes and the melt energy.

[54] **Acknowledgments.** We are grateful to the IMAU technicians, in particular Wim Boot, for the dedicated maintenance of the AWS and to several colleagues for their assistance in the field. The Norwegian Meteorological Institute is thanked for access to and use of their meteorological database eKlima. We thank the reviewers and the members of the IMAU Ice and Climate Group for valuable comments on earlier versions of the manuscript. This project has been supported by NWO (Netherlands Organisation for Scientific Research) through the Spinoza-grant to J. Oerlemans.

References

Ambach, W. (1974), The influence of cloudiness on the net radiation balance of a snow surface with high albedo, *J. Glaciol.*, *13*, 73–84.

Andreas, E. L. (1987), A theory for the scalar roughness and the scalar transfer coefficients over snow and sea ice, *Boundary Layer Meteorol.*, *38*, 159–184.

Andreassen, L. M., H. Elvehøy, B. Kjøllmoen, R. V. Engeset, and N. Haakensen (2005), Glacier mass-balance and length variation in Norway, *Ann. Glaciol.*, *42*, 317–325.

Andreassen, L. M., M. R. van den Broeke, R. H. Giesen, and J. Oerlemans (2008), A 5 year record of surface energy and mass balance from the ablation zone of Storbreen, Norway, *J. Glaciol.*, *54*, 245–258.

Arnold, N. S., W. G. Rees, A. J. Hodson, and J. Kohler (2006), Topographic controls on the surface energy balance of a high Arctic valley glacier, *J. Geophys. Res.*, *111*, F02011, doi:10.1029/2005JF000426.

Braithwaite, R. J. (1995), Aerodynamic stability and turbulent sensible-heat flux over a melting ice surface, the Greenland ice sheet, *J. Glaciol.*, *41*, 562–571.

Brock, B. W., I. C. Willis, and M. J. Sharp (2006), Measurement and parameterization of aerodynamic roughness length variations at Haut Glacier d'Arolla, Switzerland, *J. Glaciol.*, *52*, 281–297.

Curry, J. A., and P. J. Webster (1999), *Thermodynamics of Atmospheres and Oceans*, 471 pp., Academic Press, San Diego, Calif.

Denby, B., and W. Greuell (2000), The use of bulk and profile methods for determining surface heat fluxes in the presence of glacier winds, *J. Glaciol.*, *46*(154), 445–452.

Garratt, J. R. (1999), *The Atmospheric Boundary Layer*, 316 pp., Cambridge Univ. Press, New York.

Greuell, W., W. H. Knap, and P. C. Smeets (1997), Elevational changes in meteorological variables along a midlatitude glacier during summer, *J. Geophys. Res.*, *102*(D22), 25,941–25,954.

Hock, R. (2005), Glacier melt: A review of processes and their modelling, *Prog. Phys. Geogr.*, *29*, 362–391.

Hock, R., and B. Holmgren (1996), Some aspects of energy balance and ablation of Storglaciären, Northern Sweden, *Geogr. Ann. A*, *78*, 121–131.

Hock, R., and B. Holmgren (2005), A distributed surface energy-balance model for complex topography and its application to Storglaciären, Sweden, *J. Glaciol.*, *51*, 25–36.

Hurrell, J. W. (1995), Decadal trends in the North Atlantic Oscillation: Regional temperatures and precipitation, *Science*, *269*, 676–679.

Iqbal, M. (1983), *An Introduction to Solar Radiation*, 390 pp., Academic Press, New York.

Ishikawa, N., I. F. Owens, and A. P. Sturman (1992), Heat balance characteristics during fine periods on the lower parts of the Franz Josef Glacier, South Westland, New Zealand, *Int. J. Climatol.*, *12*, 397–410.

Kjøllmoen, B., L. M. Andreassen, H. Elvehøy, E. Gudevang, and M. Jackson (2001), Glaciological investigations in Norway in 2000, *NVE Report No 2*, 122 pp., Norwegian Water Resources and Energy Directorate, Oslo.

Kjøllmoen, B., L. M. Andreassen, R. Engeset, H. Elvehøy, L. P. Høivik, and M. Jackson (2003), Glaciological investigations in Norway in 2001,

NVE Report No. 2, 102 pp., Norwegian Water Resources and Energy Directorate, Oslo.

Kjøllmoen, B., L. M. Andreassen, H. Elvehøy, M. Jackson, A. M. Tvede, T. Laumann, and R. H. Giesen (2007), Glaciological investigations in Norway in 2006, *NVE Report No 1*, 99 pp., Norwegian Water Resources and Energy Directorate, Oslo.

Klemsdal, T. (1970), A glacio-meteorological study of Gråsubreen, Jotunheimen, in *Norsk Polarinstitutt - Årbok 1968*, pp. 58–74, Oslo.

Klok, E. J., and J. Oerlemans (2002), Model study of the spatial distribution of the energy and mass balance of Morteratschgletscher, Switzerland, *J. Glaciol.*, *48*(163), 505–518.

Klok, E. J., M. Nolan, and M. R. van den Broeke (2005), Analysis of meteorological data and the surface energy balance of McCall Glacier, Alaska, USA, *J. Glaciol.*, *51*(174), 451–461.

Konya, K., T. Matsumoto, and R. Naruse (2004), Surface heat balance and spatially distributed ablation modelling at Koryto Glacier, Kamchatka peninsula, Russia, *Geogr. Ann. A*, *86*, 337–348.

Konzelmann, T., and R. J. Braithwaite (1995), Variations of ablation, albedo and energy balance at the margin of the Greenland ice sheet, Kronprins Christian Land, eastern north Greenland, *J. Glaciol.*, *41*, 174–182.

Liestøl, O. (1967), Storbreen Glacier in Jotunheimen, Norway, *Tech. Rep. Nr. 141*, Norsk Polarinstitutt Skrifter, Oslo.

Messel, S. (1971), Mass and heat balance of Omnsbreen—a climatically dead glacier in southern Norway, *Tech. Rep. Nr. 156*, Norsk Polarinstitutt Skrifter, Oslo.

Meyers, T. P., and R. F. Dale (1983), Predicting daily insolation with hourly cloud height and coverage, *J. Clim. Appl. Meteorol.*, *22*, 537–545.

Mölg, T., and D. R. Hardy (2004), Ablation and associated energy balance of a horizontal glacier surface on Kilimanjaro, *J. Geophys. Res.*, *109*, D16104, doi:10.1029/2003JD004338.

Munro, D. S. (1989), Surface roughness and bulk heat transfer on a glacier: Comparison with eddy correlation, *J. Glaciol.*, *35*, 343–348.

Munro, D. S. (1990), Comparison of melt energy computations and ablatometer measurements on melting ice and snow, *Arct. Alp. Res.*, *22*, 153–162.

Oerlemans, J. (2000), Analysis of a 3 year meteorological record from the ablation zone of Morteratschgletscher, Switzerland: Energy and mass balance, *J. Glaciol.*, *46*(155), 571–579.

Oerlemans, J. (2001), *Glaciers and Climate Change*, 148 pp., Balkema, Lisse, Netherlands.

Oerlemans, J., and B. Grisogono (2002), Glacier winds and parameterisation of the related surface heat fluxes, *Tellus*, *54A*, 440–452.

Oerlemans, J., and E. J. Klok (2002), Energy balance of a glacier surface: Analysis of automatic weather station data from the Morteratschgletscher, Switzerland, *Arct. Antarct. Alp. Res.*, *34*(4), 477–485.

Reichert, B. K., L. Bengtsson, and J. Oerlemans (2001), Midlatitude forcing mechanisms for glacier mass balance investigated using general circulation models, *J. Clim.*, *14*, 3767–3784.

Smeets, C. J. P. P. (2006), Assessing unaspirated temperature measurements using a thermocouple and a physically based model, in *The Mass Budget of Arctic Glaciers, Extended abstracts—Workshop and GLACIODYN Planning Meeting 2006*, pp. 99–101, Institute for Marine and Atmospheric Research Utrecht, Utrecht, Netherlands.

Strasser, U., J. Corripio, F. Pellicciotti, P. Burlando, B. Brock, and M. Funk (2004), Spatial and temporal variability of meteorological variables at Haut Glacier d'Arolla (Switzerland) during the ablation season 2001: Measurements and simulations, *J. Geophys. Res.*, *109*, D03103, doi:10.1029/2003JD003973.

Van den Broeke, M. R., C. H. Reijmer, and R. S. W. van de Wal (2004), Assessing and improving the quality of unattended radiation observations in Antarctica, *J. Atmos. Oceanic Technol.*, *21*(9), 1417–1431.

Van den Broeke, M. R., C. H. Reijmer, D. van As, R. S. W. van de Wal, and J. Oerlemans (2005), Seasonal cycles of Antarctic surface energy balance from automatic weather stations, *Ann. Glaciol.*, *41*, 131–139.

Van den Broeke, M. R., C. H. Reijmer, D. van As, and W. Boot (2006), Daily cycle of the surface energy balance in Antarctica and the influence of clouds, *Int. J. Climatol.*, *26*, 1587–1605.

Wagnon, P., P. Ribstein, B. Francou, and B. Pouyaud (1999), Annual cycle of energy balance of Zongo Glacier, Cordillera Real, Bolivia, *J. Geophys. Res.*, *104*(D4), 3907–3923.

Willis, I. C., N. S. Arnold, and B. W. Brock (2002), Effect of snowpack removal on energy balance, melt and runoff in a small supraglacial catchment, *Hydrol. Processes*, *16*, 2721–2749.

L. M. Andreassen, Section for Glaciers, Snow and Ice, Norwegian Water Resources and Energy Directorate, P.O. Box 5091, Majorstua, N-0316 Oslo, Norway.

R. H. Giesen, J. Oerlemans, and M. R. van den Broeke, Institute for Marine and Atmospheric Research Utrecht, Utrecht University, Princetonplein 5, NL-3584 CC Utrecht, Netherlands. (r.h.giesen@uu.nl)